(Received 24 September 2024, Accepted 5 November 2024, Scheduled 28 November 2024)

# A Technique for Alternating Generation of Single and Multi-Beams from Circularly Polarized Antenna Arrays

David Pouhè*

*School of Engineering, Reutlingen University of Applied Sciences, Alteburgstrasse 150, D-72762, Reutlingen, Germany*

**ABSTRACT:** A simple technique for generating single and multiple beams from antenna arrays is presented. The approach is based on the multistage sequential rotation technique. A new feature in using multistage sequential rotation is provided. It is demonstrated that by applying a controlled second sequential rotation, circularly polarized antenna arrays operating alternately in a single-beam mode M1 and multi-beam mode M2 in the same frequency band can be designed. Proof-of-concept is provided mathematically and through numerical simulations in light of case studies. The approach can not only be applied to large antenna arrays following a modular principle adapted to the array size and needed applications without loss of generality, but also paves the way for the manufacture of circularly polarized antennas operating alternately or simultaneously in both modes in the same frequency band. In addition, antennas designed using the proposed approach may have a wide range of applications ranging from monopulse radar to antennas for the compensation of interference and blockage in dynamic communication environments.

## 1. INTRODUCTION

Sequential rotation technique (SRT) is a well-established approach that is used to design circularly polarized antenna arrays [1, 2]. Apart from multiple-arm spiral antennas, where it has been applied to generate conical modes [3], the application of sequential rotation is focused but not limited in most studies on obtaining circularly polarized single-beam radiation from linearly/elliptical polarized radiating elements, to improve the axial ratio of circularly polarized antennas [4], broaden the bandwidth, enhance the CP purity, and achieve high gain [5, 6], and reduce mutual coupling between radiating elements and within the feed as well [7–9]. Discussions on drawbacks such as the excitation of grating lobes along with measures to improve the characteristics of the antenna are also part of existing studies [4–9]. However, this technique can also be used to develop antennas with multiple-beam radiation for applications ranging from satellite communications to improve coverage of multiple areas to radar systems to track multiple targets and mobile communications for multicasting support. Moreover, SRT can help us develop antennas that alternately generate both single- and multi-beams. This work intends to demonstrate that.

In particular, the paper aims at generalizing the approach developed in [10]. For completeness, "short-cuts" adopted in our discussion in [10] are avoided. Nevertheless, some parts of [10] are reproduced in Section 2 not only to ensure a smooth and continuous reading from one section to another but also to provide readers with a comprehensive discussion about the "ins and outs" of the method by imparting deep insights into the physics behind the approach being presented. The method is based on the multistage sequential rotation technique (MSRT) and allows the design of antennas operating in both single-beam and multi-beam modes in the same frequency range. Section 3 is devoted to the mathematical proof of the concept.

The nature of the engineering sciences is the enlightening of scientific realizations with respect to their technical applicability and practical conversion. This work would not have been completed without a reference to the practical applicabilities of the approach. Section 4 is therefore directed towards some simulated case studies to demonstrate the validity of the concept and its applicability as well. Concluding remarks round off the work in Section 5.

Throughout the work, considerations such as the type of radiating elements, the influence of distance, the mutual coupling between elements, and the gain of the antenna are considered peripheral aspects and treated as such.

## 2. THE TECHNIQUE

Consider the antenna array sketched in Fig. 1 consisting of four identical elements. The array elements are sequentially rotated. That is, they are arranged in a rectangular grid fashion with element angular orientation and feeding phase $0°$, $90°$, $180°$, $270°$.

### 2.1. Circular Polarization of the Basic Element

Suppose that each element's excitation amplitude is constant and identical; let $E^h(\vartheta, \varphi)$ be the horizontal radiated electrical field in the far field region and $E^v(\vartheta, \varphi)$ its vertical counterpart. The total radiated field $E(\vartheta, \varphi)$ in the $xy$-plane is [1]

* Corresponding author: David Pouhè (david.pouhe@reutlingen-university.de).

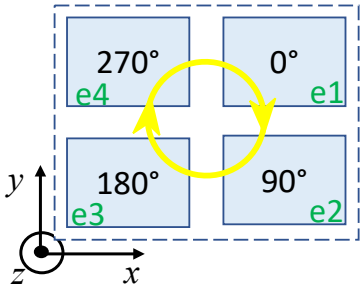


**FIGURE 1**. Sequentially rotated array of $2 \times 2$-elements for generating a circularly polarized field. The yellow circular arrow indicates the sense of rotation. $e1$, $e2$, $e3$, and $e4$ are element numbering.

$$\begin{aligned} E(\vartheta,\varphi) &= E^h_{e1}(\vartheta,\varphi)\cdot e^{-jk_0\sin\vartheta}\cdot e^{j0^\circ} + E^v_{2e}(\vartheta,\varphi)\cdot e^{jk_0\sin\vartheta}\cdot e^{j90^\circ} + E^h_{e3}(\vartheta,\varphi)\cdot e^{jk_0\sin\vartheta}\cdot e^{j180^\circ} \\ &\quad + E^v_{e4}(\vartheta,\varphi)\cdot e^{-jk_0\sin\vartheta}\cdot e^{j270^\circ} \\ &= E^h_{e1}(\vartheta,\varphi)\cdot e^{-jk_0\sin\vartheta}\cdot e^{j0^\circ} - E^h_{e3}(\vartheta,\varphi)\cdot e^{jk_0\sin\vartheta}\cdot e^{j0^\circ} + E^v_{e2}(\vartheta,\varphi)\cdot e^{jk_0\sin\vartheta}\cdot e^{j90^\circ} \\ &\quad - E^v_{e4}(\vartheta,\varphi)\cdot e^{-jk_0\sin\vartheta}\cdot e^{j90^\circ} \\ &= E^h_{e1}(\vartheta,\varphi)\left(e^{-jk_0\sin\vartheta} - e^{jk_0\sin\vartheta}\right)\cdot e^{j0^\circ} + E^v_{e2}(\vartheta,\varphi)\left(e^{-jk_0\sin\vartheta} - e^{jk_0\sin\vartheta}\right)\cdot e^{j90^\circ} \\ &= 2j\left[E^h_{e1}(\vartheta,\varphi)\cdot e^{j0^\circ} + E^v_{e2}(\vartheta,\varphi)\cdot e^{j90^\circ}\right]\cdot\sin(k_0\sin\vartheta) \end{aligned} \tag{1}$$

since $E^h_{e1} = E^h_{e3}$ and $E^v_{e2} = E^v_{e4}$.

The expression $E^h_{e1}(\vartheta,\varphi)\cdot e^{j0^\circ} + E^v_{e2}(\vartheta,\varphi)\cdot e^{j90^\circ}$ is a pure circularly polarized wave, while $\sin(k_0\sin\vartheta)$ represents the array factor. $k_0$ is the wave number; $E_{e1}$, $E_{e2}$, $E_{e3}$, and $E_{e4}$ are respectively the field radiated by elements $e1$, $e2$, $e3$, and $e4$.

We can now use it as a basic element for the antenna configurations in the following and turn attention to the description of the technique.

### 2.2. Description of the Technique

The technique presented here comprises two main steps: the design of the initial antenna and the direct application of the first sequential rotation as the first step. The second step is physically rotating the basic subarrays to obtain an arrangement in which each subgroup is orthogonal to its subsequent one and then applying a controlled second sequential rotation in the same sense of rotation as the first one and in the reversed sense.

*1) Step* 1*: The Initial Antenna Array Configuration A1:* The $2 \times 2$-elements array is duplicated twice in the $x$- and $y$-directions to obtain the array displayed in Fig. 2, which is a 16-element array organized as $4 \times 4$ identical $2 \times 2$ element subarrays. This configuration is named initial array configuration A1 assembled from subgroups. For convenience, we assign each subarray an index $i$, where $i = 1, 2, 3, 4$ (Fig. 2).

From Fig. 2, it is seen that this sequential rotation scheme provides co-polarization in the center of the antenna and maintains it in each subarray. Hence, co-polarization is along the main diagonals, and a large part of the field energy will be concentrated in the desired copolar component, despite the existence of cross-polarisation at some points on the planes $\varphi = 0^\circ$ and $\varphi = 90^\circ$. Array A1 radiates a circularly polarized field in the broadside direction. This radiation mode is named mode M1 radiation.

*Step* 2*: Physical Rotation of the Basic Elements and Application of a Controlled Second Sequential Rotation:* The basic elements are now arranged such that each subgroup is perpendicular to the subsequent element to obtain array A2 (Fig. 3). That is, a physical rotation of a subarray $i$ by $90^\circ$ with respect to the new position of subarray $i-1$ is performed. Precisely, subarray 2 has been physically rotated by $90^\circ$ around its perpendicular axis. A further rotation of subgroup 2 by $90^\circ$ gives the phase relationship on subarray 3, which from its new position is rotated by $90^\circ$ to obtain the phase relationship on subarray 4. In other words, subgroup 3 is rotated by $180^\circ$ and subarray 4 by $270^\circ$ around their respective orthogonal axis. The rotations are counterclockwise in the present case but may also be clockwise. This arrangement increases the isolation between feeding network ports, provided that each subarray has an isolated feed with a central feeding point.

The application of a second sequential rotation (SSR) in the same sense as the first one (black circular arrows in Fig. 4(a)) and with a phase difference of $90^\circ$ between two consecutive subarrays leads to an identical polarization state and sense as in the initial case (Fig. 4(b)). That is seen by comparing the phase relationship on radiating elements in Figs. 2 and 4(b). Hence, the antenna operates in Mode M1.

In fact, circular polarization is maintained at the center of the antenna and in each subarray after the SSR, which is logical since each subarray has perfect circular polarization [7]. However, the upright preservation of the co-polarization in the center of the antenna after the SSR in the first case (Fig. 4) is mainly because the SSR is in the same sense as the first one.

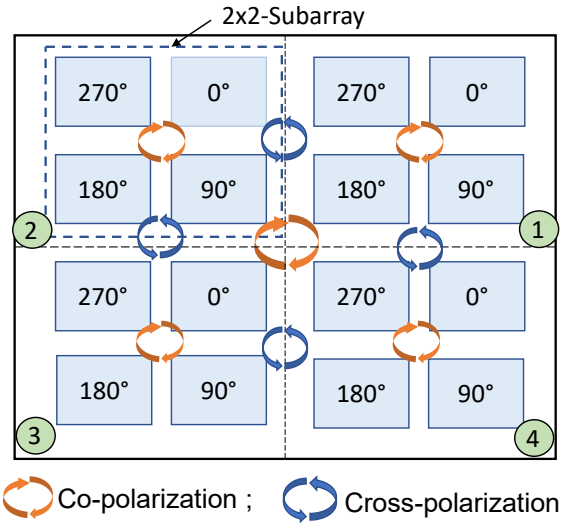


**FIGURE 2**. Initial antenna A1. Phase relationship on the antenna's radiating elements and sense of the circular polarization. The subarrays are numbered 1, 2, 3, and 4.

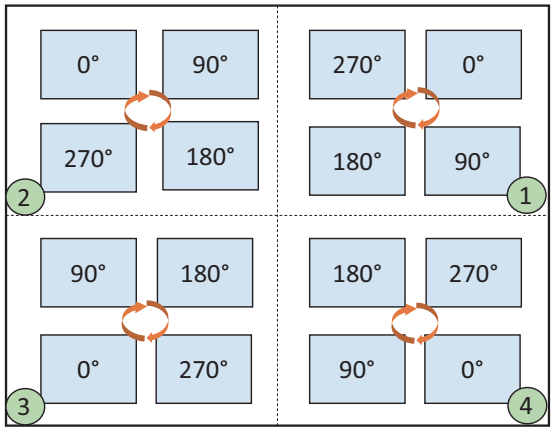


**FIGURE 3**. Phase relationship on the radiating elements of antenna A2.

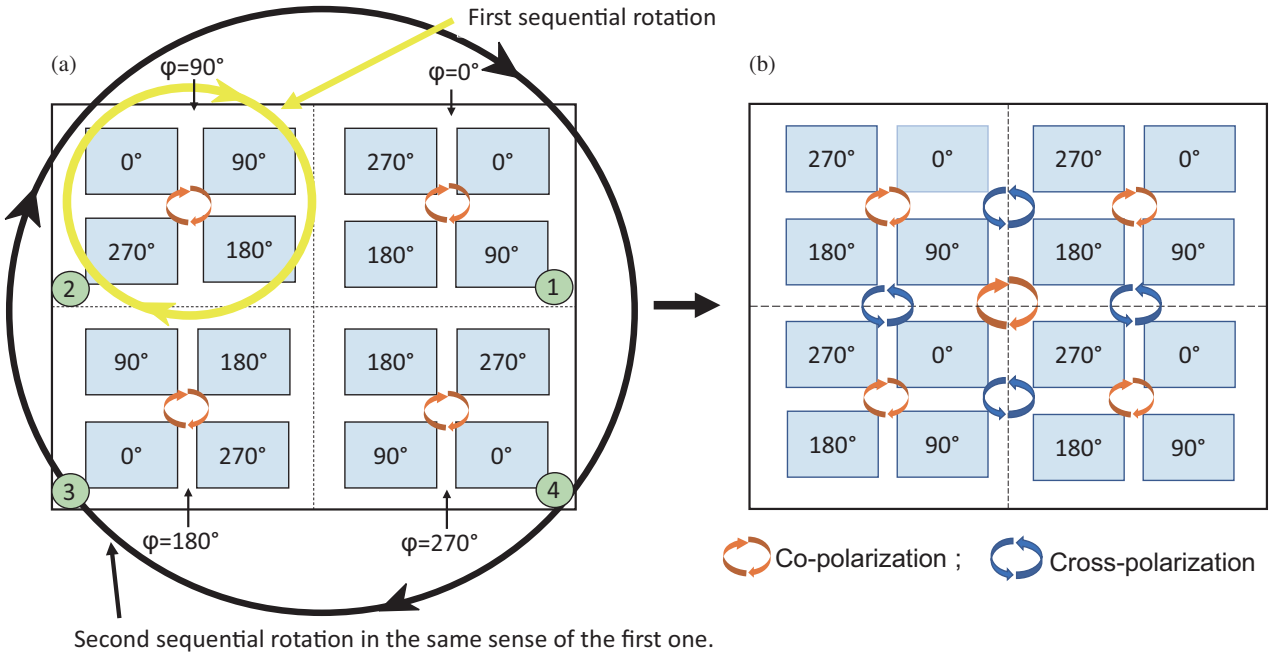


**FIGURE 4**. (a): Application of the second sequential rotation in the same sense as the first one on antenna A2 and (b): obtained phase relationship on the radiating elements.

Along the median (the center of the antenna excluded), cross-polarization dominates (Fig. 4(b)). As a consequence, higher side lobe levels (SLLs) due to potential grating lobes are expected for large arrays in planes $\varphi = 0°$ and $\varphi = 90°$.

Co-polarization is maintained on each subarray by reversing the sense of the SSR (blue circular arrows in Fig. 5(a)). At the same time, cross-polarization is formed in the center of the antenna, indicating a nullification of the copolar field. Off the broadside, along the planes $\varphi = 0°$ and $\varphi = 90°$, co- and cross-polarizations are mutually exclusive. Zeros or fields close to zero appear along these planes (Fig. 5(b)). As a result, the antenna radiates in a conical mode called M2-Mode, which has four main beams. The radiated field is circularly polarized in the direction of main radiations since the circular polarization is maintained in each subarray.

Off the broadside and along the medians, zero field appears if and only if the co- and cross-polar fields are of equal intensities; otherwise, the field is much lower along these lines than the field in the boresight directions. This insight underpins the fact that, when the sense of the SSR is reversed, the antenna operates in a conical mode modus.

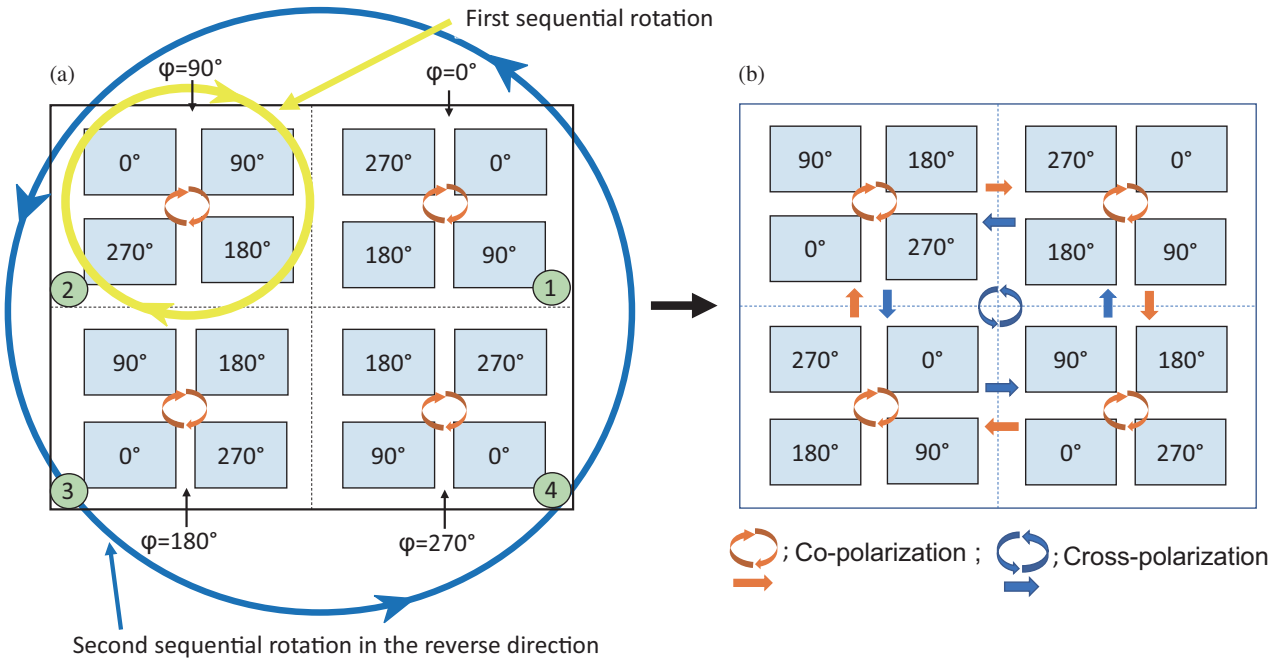


**FIGURE 5**. (a): Application of the second sequential rotation in the reverse sense of the first one on antenna A2 and (b): obtained phase relationship on the radiating elements.

It is noteworthy that, regardless of its sense of rotation, the SSR has no influence on the polarization hand.

From the above demonstration, it is clear that antenna A2 can operate in two different modes in the same frequency band: M1 mode with radiation orthogonal to the antenna plane and/or conical radiation mode M2 with several equal beams. The number of conical beams depends on the number of subarrays and their arrangement in groups of four subarrays. This grouping, in turn, is a function of the number of conical beams needed. In the present case, where the antenna is subdivided into four subgroups, four main beams of equal intensity are radiated.

## 3. MATHEMATICAL PROOF-OF-CONCEPT

For the mathematical proof of the described technique, we use Eq. (A2) in [13] for multistage sequential rotation.

Assuming right hand circular polarization (RHCP) to be the co-polarized component and the same excitation for all antenna elements, Eq. (A2) in [13] can be rewritten as

$$\begin{aligned}\mathbf{E}_T &= \sum_{m=1}^{4}\sum_{n=1}^{4}\frac{e^{-jk_0 r_{m,n}}}{r_{m,n}}\mathbf{E}_{m,n}\\ &\approx \frac{e^{-j(k_0 r_{1,1}-\beta_{11}+\varphi_{1,1})}}{r}\sum_{m=1}^{4}\sum_{n=1}^{4}e^{j[-k_0[(m-1)d_x\cdot u+(n-1)d_y\cdot v]+(\beta_{mn}-\beta_{11})+(\varphi_{11}-\varphi_{mn})]}\cdot\mathbf{e}_R\\ &\quad+\frac{e^{-j(k_0 r_{1,1}-\beta_{11}-\varphi_{1,1})}}{r}\sum_{m=1}^{4}\sum_{n=1}^{4}\sqrt{p_{ele}}e^{j[-k_0[(m-1)d_x\cdot u+(n-1)d_y\cdot v]+(\beta_{mn}-\beta_{11})+(\varphi_{mn}-\varphi_{11})]}\cdot\mathbf{e}_L\end{aligned} \tag{2}$$

In Eq. (2),

$u = \sin\vartheta\cos\varphi$; $v = \sin\vartheta\sin\varphi$

$r_{mn}$ = distance between the observation point and ($m^{th}$, $n^{th}$)-element,

$r$ = distance between the observation point and the geometrical center of the array,

$d_x$ and $d_y$ are the inter-element spacing. In our particular case, it is assumed that $d_x = d_y = d$,

$\beta_{mn}$ = excitation phase of the element,

$\varphi_{mn}$ = orientation angle of the element,

$\mathbf{e}_R = \frac{1}{\sqrt{2}}(\mathbf{e}_\varphi + j\mathbf{e}_\vartheta)$ and $\mathbf{e}_L = \frac{1}{\sqrt{2}}(\mathbf{e}_\varphi - j\mathbf{e}_\vartheta)$ are the unit vectors of the RHCP and LHCP waves respectively.

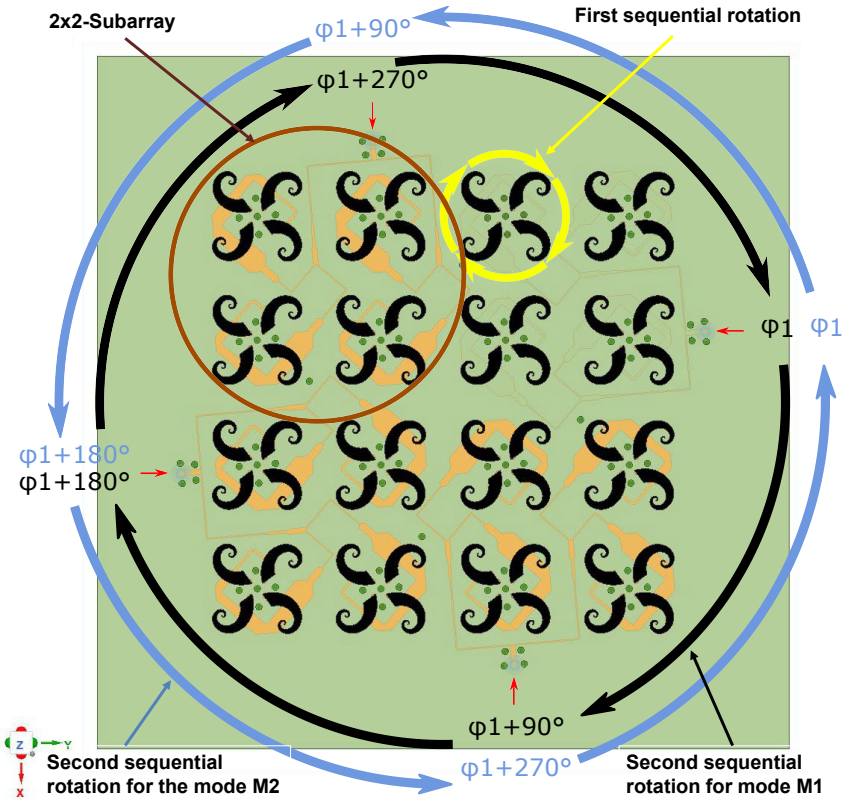


**FIGURE 6**. Designed $4 \times 4$ DCSA-array with an illustration of the sense of the sense of sequential rotation for modes M1 and M2. The yellow circular arrows indicate the sense of rotation in the single element. Black circular arrows show the rotation sense for mode M1, while blue circular arrows delineate the rotation sense for mode M2.

$p_{ele}$ is the cross-polarization level of each element ($0 < p_{ele} < 1$).

Since the 16-element array is organized as $4 \times 4$ identical $2 \times 2$ element subarrays in a rectangular fashion of 2 rows and 2 columns, the total electric field may be expressed as

$$\begin{aligned}
\mathbf{E}_T &= \sum_{m=1}^{2}\sum_{n=1}^{2} \frac{e^{-jk_0 r_{m,n}}}{r_{m,n}} \mathbf{E}_{m,n} \\
&\approx \frac{e^{-j(k_0 r_{1,1} - \beta_{11} + \varphi_{1,1})}}{r} \left\{ 1 + e^{j[-k_0 d_y \cdot v + (\beta_{12} - \beta_{11}) + (\varphi_{11} - \varphi_{12})]} + e^{j[-k_0 d_x \cdot u + (\beta_{21} - \beta_{11}) + (\varphi_{11} - \varphi_{21})]} \right. \\
&\quad \left. + e^{j[-k_0 (d_x u + d_y v) + (\beta_{22} - \beta_{11}) + (\varphi_{11} - \varphi_{22})]} \right\} \cdot \mathbf{e}_R \\
&\quad + \frac{e^{-j(k_0 r_{1,1} - \beta_{11} - \varphi_{1,1})}}{r} \left\{ \sqrt{p_{ele}} \left[ 1 + e^{j[-k_0 d_y \cdot v + (\beta_{12} - \beta_{11}) + (\varphi_{12} - \varphi_{11})]} + e^{j[-k_0 d_x \cdot u + (\beta_{21} - \beta_{11}) + (\varphi_{21} - \varphi_{11})]} \right. \right. \\
&\quad \left. \left. + e^{j[-k_0 (d_x u + d_y v) + (\beta_{22} - \beta_{11}) + (\varphi_{22} - \varphi_{11})]} \right] \right\} \cdot \mathbf{e}_L
\end{aligned} \tag{3}$$

To obtain Eq. (3), we have simplified the 16-element array to an array of $2 \times 2$ element subarrays, where each subgroup is a sequentially rotated element, and a matrix indexing of the elements was adopted.

### 3.1. Physical Rotation of the Elements and Application of the Second Sequential Phased Rotation

A physical rotation of the basic elements as described in Subsubsection 2.2 and application of a second sequential rotation in the same sense as for the first one with a phase difference of 90° between two adjacent elements leads to

$$\begin{aligned}
\mathbf{E}_T &= \frac{e^{-jk_0 r_{11}}}{r} \left\{ 1 + e^{-jk_0 dv} + e^{-jk_0 du} + e^{-jk_o d(u+v)} \right\} \mathbf{e}_R \\
&\quad + \frac{e^{-jk_0 r_{11}}}{r} \left\{ \sqrt{p_{ele}} \left[ 1 + e^{j(-k_0 dv + 180°)} \right. \right. \\
&\quad \left. \left. + e^{j(-k_0 du + 540°)} + e^{j[-k_0 d(u+v) + 360°]} \right] \right\} \mathbf{e}_L
\end{aligned} \tag{4}$$

Bearing in mind that 360° coincide with 0° and 540° with 180°, Eq. (4) may be rewritten as

$$\mathbf{E}_T = \frac{e^{-jk_0r_{11}}}{r}\left\{1+e^{-jk_0dv}+e^{-jk_0du}+e^{-jk_od(u+v)}\right\}\mathbf{e}_R + \frac{e^{-jk_0r_{11}}}{r}\left\{\sqrt{p_{ele}}\left[1+e^{j(-k_0dv+180^\circ)} + e^{-jk_0d(u+v)}+e^{j(-k_0du+180^\circ)}\right]\right\}\mathbf{e}_L \quad (5)$$

From Eq. (5), it is seen that there is no additional instantaneous phase progression in the far-field phase between adjacent copolar components, which suggests that the second sequential rotation either has no influence on the phase progression of the copolar field after the first sequential rotation or only reinforces it. The cross-polar field on its side shows a phase progression of 180° between adjacent components, resulting in a zero cross-polar field in the broadside direction. In fact, the excitation phase equals minus the orientation angle of the element ($\beta_i = -\varphi_i$). As a result, the cross-polar field components are canceled out, yielding a directive copolar beam [2, 14]. The antenna therefore operates in mode M1-radiation.

Reversing now the sense of the second sequential rotation yields

$$\mathbf{E}_T = \frac{e^{-jk_0r_{11}}}{r}\left\{1+e^{-jk_0dv+180^\circ} + e^{-jk_0du-180^\circ}+e^{-jk_od(u+v)}\right\}\mathbf{e}_R + \frac{e^{-jk_0r_{11}}}{r}\left\{\sqrt{p_{ele}}\left[1+e^{j(-k_0dv+360^\circ)} + e^{j(-k_0du+360^\circ)}+e^{j[-k_0d(u+v)+360^\circ]}\right]\right\}\mathbf{e}_L \quad (6)$$

which by considering that 360° coincide with 0° may be rewritten as

$$\mathbf{E}_T = \frac{e^{-jk_0r_{11}}}{r}\left\{1+e^{-jk_0dv+180^\circ} + e^{-jk_od(u+v)}+e^{-jk_0du-180^\circ}\right\}\mathbf{e}_R + \frac{e^{-jk_0r_{11}}}{r}\left\{\sqrt{p_{ele}}\left[1+e^{-jk_0dv} + e^{-jk_0du}+e^{-jk_0d(u+v)}\right]\right\}\mathbf{e}_L \quad (7)$$

Equation (7) shows that apart from the phase due to $k_0du$, $k_0dv$ and $k_0d(u+v)$, there is an additional phase progression of 180° between the copolar field components, which, following considerations about four-arm spiral antennas, together with the fact that for $\beta_i = \varphi_i$ the copolar field becomes zero along the broadside direction, suggests radiation of the conical mode M2 with four main beams, a null along the axis orthogonal to the antenna plane, rotation symmetry about the boresight axis, and circular polarization [3].

The approach thus presented paves the way for the manufacture of circularly polarized antennas operating alternately in both modes in the same frequency band, as demonstrated in the next section in light of case studies.

## 4. CASE STUDIES

The technique described above was applied to different antenna arrays: the broadband antenna for satellite communication presented in [15], the double cornu-spiral antenna (DCSA) [16], and the spiral antenna arrays investigated in [17]. However, because of the space limitation, only simulated results for the broadband antenna for the DCSA using ANSYS-HFSS are presented below. Results for the broadband antenna for satellite are found in [10]. Details on radiation characteristics, such as the gain of the respective basic elements and arrays thereof, can be found in cited sources and will not be repeated here. Instead, we will put emphasis on the radiation patterns and axial ratios. Nevertheless, peripheral aspects of this work, such as the isolation between input ports and the reflection coefficient, are mentioned.

The array of 2 × 2-elements in [16] was duplicated twice in the $x$- and $y$-directions yielding a 4 × 4-elements array of DCSA in which the array of 2 × 2-elements is a subarray (Fig. 6). Each 2 × 2-subarray has the 0°, 90°, 180°, 270° element angular and phase arrangements (Fig. 7). Fig. 8 shows the phase relationship on radiating elements after rotation of subarrays 2, 3, and 4 as described in Step 2 (Subsection 2.2). The overall

| | | | |
|---|---|---|---|
| 90° | 180° | 0° | 90° |
| 0° | 270° | 270° | 180° |
| 90° | 180° | 0° | 90° |
| 0° | 270° | 270° | 180° |

**FIGURE 7**. Phase relationship on the radiating elements of the basic 2 × 2-subarray element.

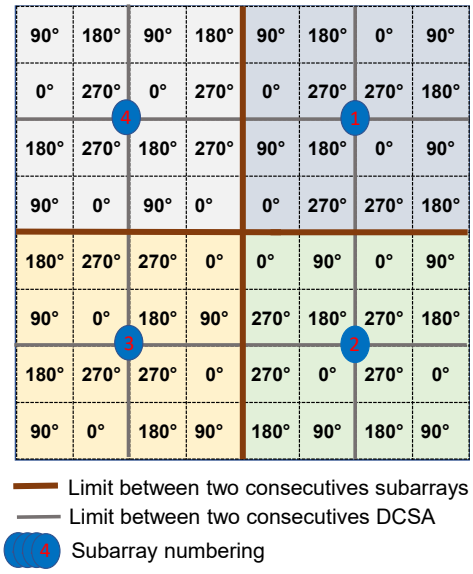


**FIGURE 8**. Phase relationship on the radiating elements of the 4 × 4-array after rotation of subgroups 2, 3 and 4 as described in Subsection 2.2. The rotation was clockwise.

dimensions of the antenna are $64.5 \times 64.5 \times 2.453$ mm. The distance between two adjacent radiating elements in the $x$ and $y$ directions was $d_x = d_y = d = \lambda/4$, where $\lambda$ is the wavelength at the operation frequency (24 GHz). Simulations have been carried out by applying the approach presented in Section 2.2.

Figures 9 and 10 display the phase relationship on radiating elements and sense of the circular polarization after the application of the two-stage sequential rotation for modes M1 and M2, respectively. As can be seen from Fig. 9, co-polarization is obtained in the center of the array and along the whole diagonals (main and secondary) of the array structure, while in the principal planes ($\varphi = 0°$ and $\varphi = 90°$), as well as the planes parallel them, co-polarization and cross-polarization alternate. Radiation patterns can be considered a superposition of co- and cross-polarizations at each angle in the elevation direction. In particular, side lobes contain energy components from co- and cross-polar fields. This is substantiated in Fig. 11 where radiation patterns at different frequencies are presented.

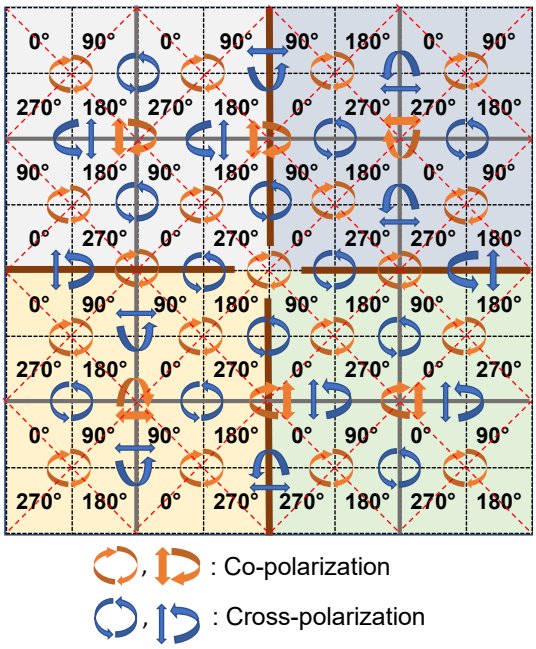


**FIGURE 9**. Phase relationship on radiating elements and illustration of the sense of the circular polarization after application of the two-stage rotation for mode M1 radiation. Along the diagonals, we have co-polarization. On the $\varphi = 0°$ and $\varphi = 90°$ planes, as well as the planes parallel to these two planes, co-polarization and cross-polarization alternate.

The influence of the sequential rotation and MSR as described in the previous sections but also in the literature [1, 2, 4, 6–14] are well appreciated by observing the radiation characteristics (Figs. 11 to 16). Especially the input ports are decoupled from each other (Fig. 13); the axial ratio (Figs. 14, 15) is improved in magnitude, frequency, and angular range compared to the $2 \times 2$-elements array. The polarization is RHCP with a high degree of polarization purity in the boresight direction over a large bandwidth (Fig. 16). Sidelobe levels are enhanced as expected. SLLs of $-11.054$ dB in the principal planes ($\varphi = 0°$ and $\varphi = 90°$) are recorded at angles

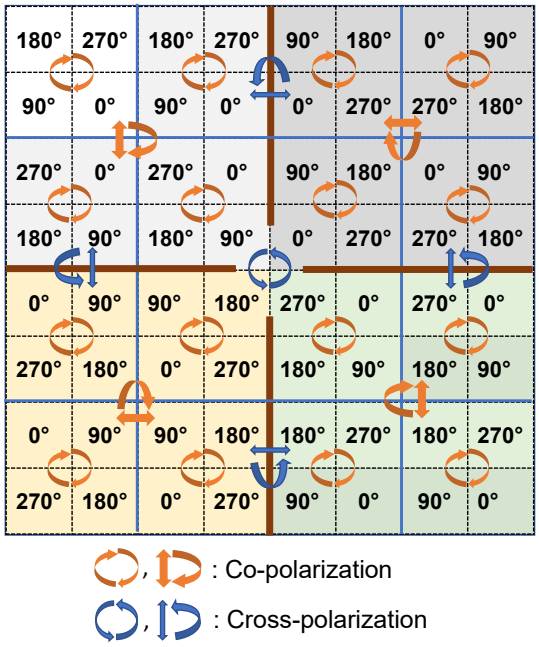


**FIGURE 10**. Phase relationship on radiating elements and illustration of the circular polarization's sense after applying the two-stage sequential rotation for mode M2 radiation.

immediately off the broadside direction as can be seen from Fig. 11 where the radiation patterns at 22, 24, 25, and 26 GHz are displayed. At oblique cut planes, $\varphi = 45°$ and $135°$ the SLLs are much lower: $SLL_{max} = -18.81$ dB at $f = 24$ GHz. This is a consequence of the double sequential rotation. Along the cut-planes $\varphi = 45°$ and $\varphi = 135°$ and in planes parallel to them, co-polarization is along the whole diagonals (Fig. 9), and a large part of the field energy is concentrated in the desired copolar component, which leads to low SLLs.

On the $\varphi = 0$ and $\varphi = 90$ planes and the planes parallel to them, co-polarization and cross-polarization alternate (Fig. 9). This induces high SLLs at some elevation angles, as shown in Fig. 11.

Mode M2 radiation is obtained by reversing the sense of the second sequential rotation according to the rotation sense of the blue arrow (Fig. 6). Again, the antenna shows good radiation characteristics. The phase reversion affects neither the reflection coefficient nor the coupling between ports. They are identical to the reflection coefficient and isolation between ports in the mode M1 case. The axial ratio (Fig. 17) and radiation pattern (Figs. 18 and 19) change however.

The antenna exhibits mode M2 pattern with four main beams pointing in different directions simultaneously, a sharp on-axis null and rotational symmetry about the broadside axis (Fig. 18). Maximal radiation occurs at $\varphi = \pm 45°, \pm 135°$. 2D-radiation pattern diagrams are therefore only presented along these planes. Figs. 19 shows the corresponding pattern at different frequencies. The null at the boresight axis is visible, especially at 21 and 22 GHz.

Note that slight deviations in the amplitude of the radiation patterns were observed at some off-resonance frequencies.

The cross-polar discrimination is displayed in Fig. 20. Obviously, changing the sense of the second sequential rotation

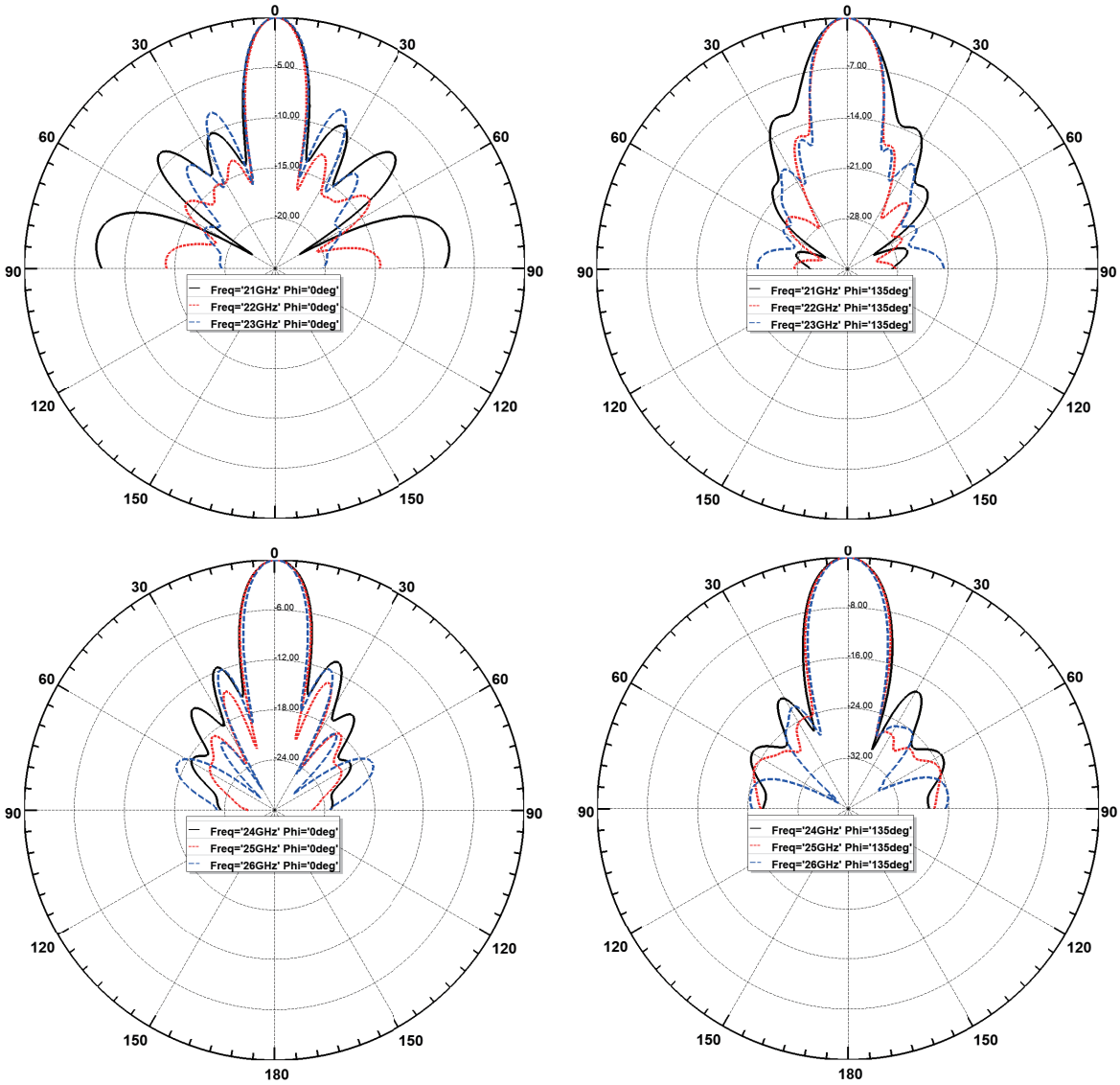


**FIGURE 11**. Normalized radiation pattern at 21, 22 and 23 24, 25, and 26 GHz for mode M1. Because of the rotational symmetry of the radiation pattern about the broadside axis, only patterns at $\varphi = 0^\circ$ and $\varphi = 135^\circ$ are displayed. Similar results were obtained in orthogonal planes, $\varphi = 90^\circ$ and $\varphi = 45^\circ$.

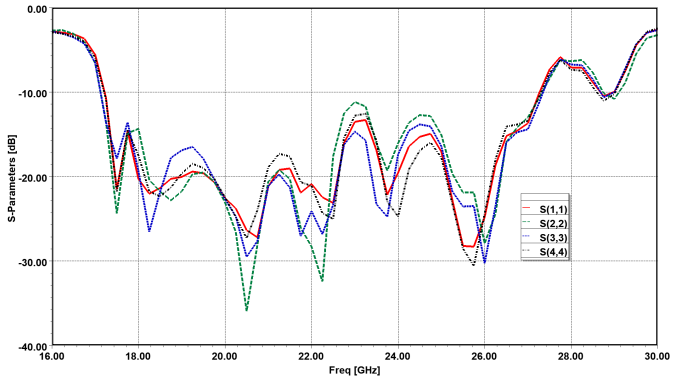


**FIGURE 12**. Input reflexion coefficients. The impedance bandwidth of the antenna is identical to that of the $2 \times 2$-elements array.

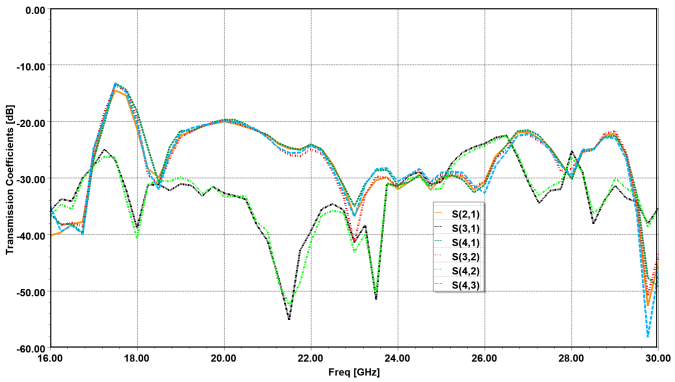


**FIGURE 13**. Port-to-port coupling. The ports are well isolated from each other.

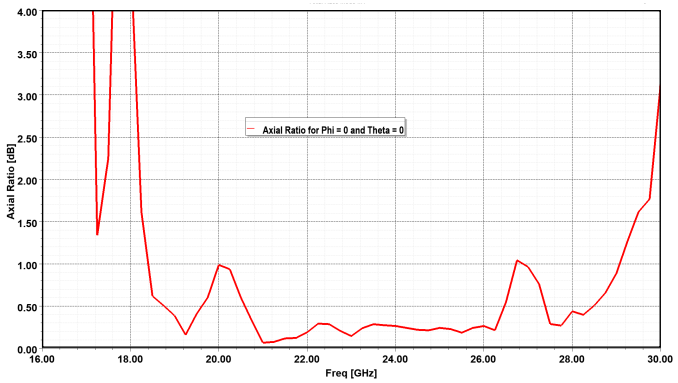


**FIGURE 14**. Axial ratio versus frequency for mode M1.

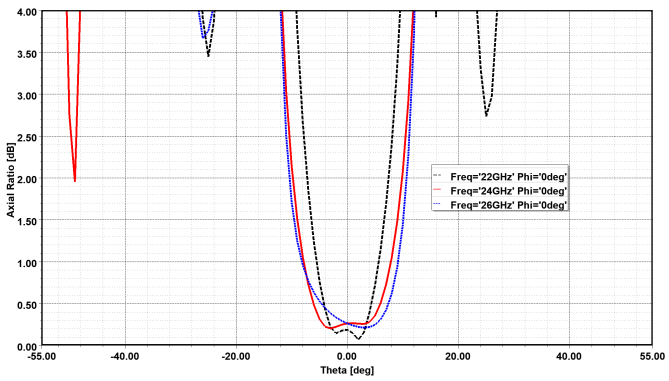


**FIGURE 15**. Axial ratio versus angle for mode M1.

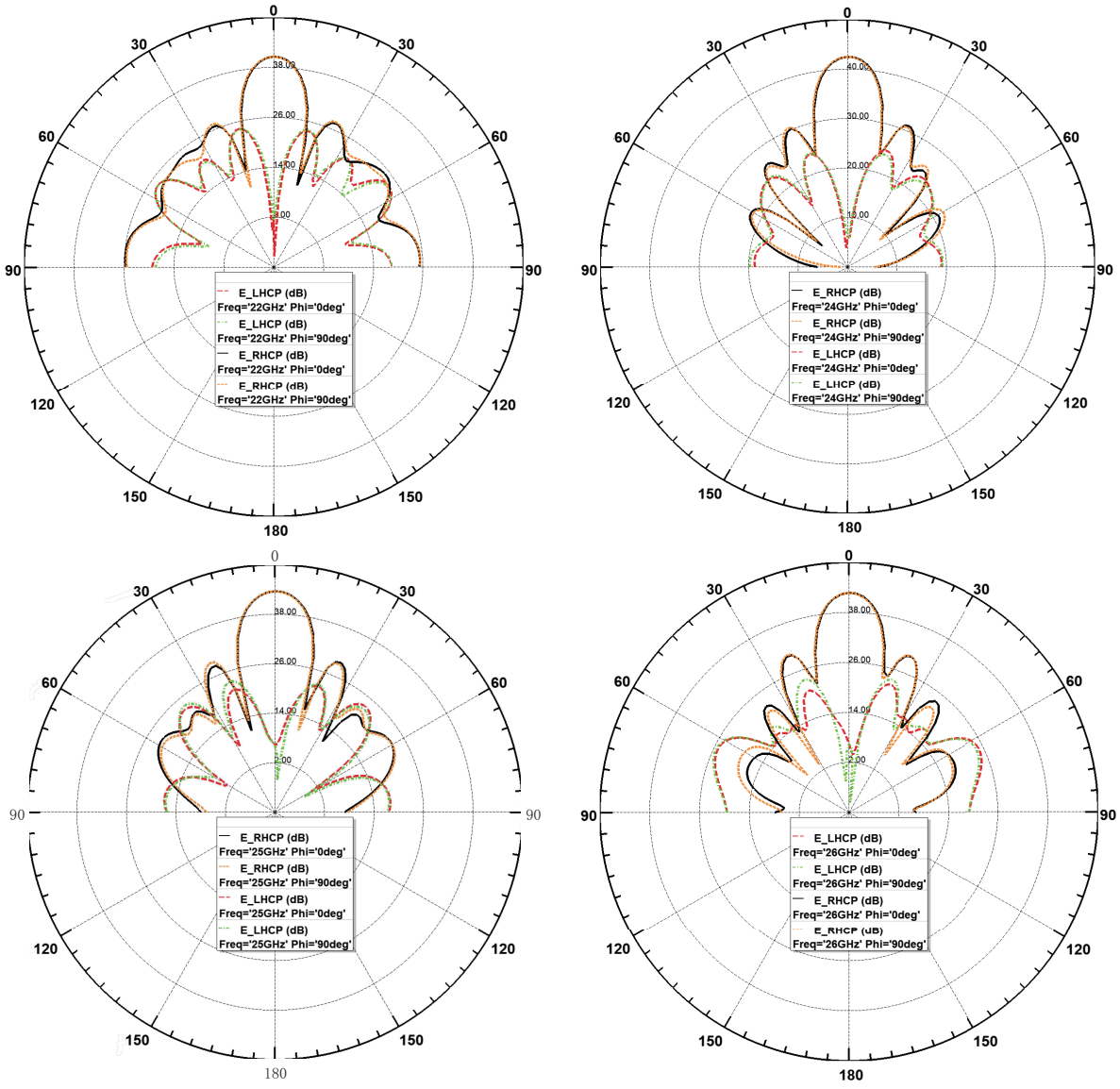


**FIGURE 16**. Cross polar discrimination for mode M1 operation at 22, 24, 25, and 26 GHz. The XPD for all frequencies is at least 36 dB at $\vartheta = 0$. The antenna is right-hand circular polarized.

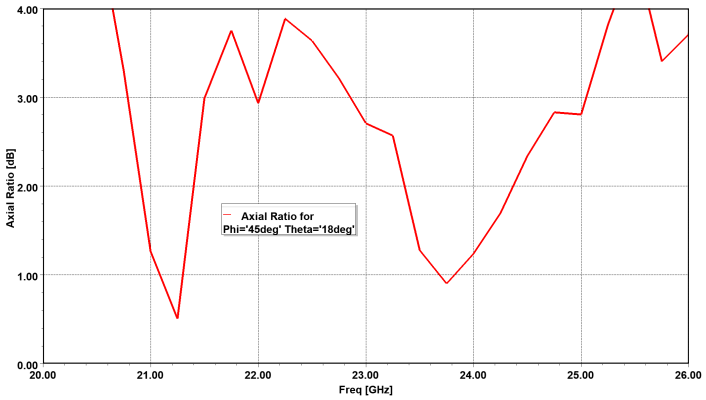


**FIGURE 17**. Axial ratio versus frequency for mode M2.

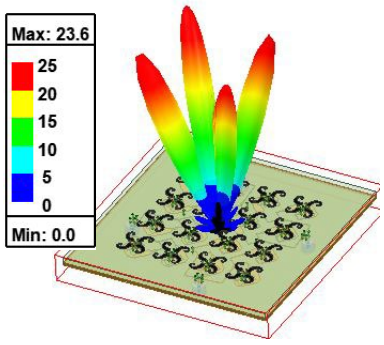


**FIGURE 18**. 3D-radiation pattern of the antenna in mode M2 operation.

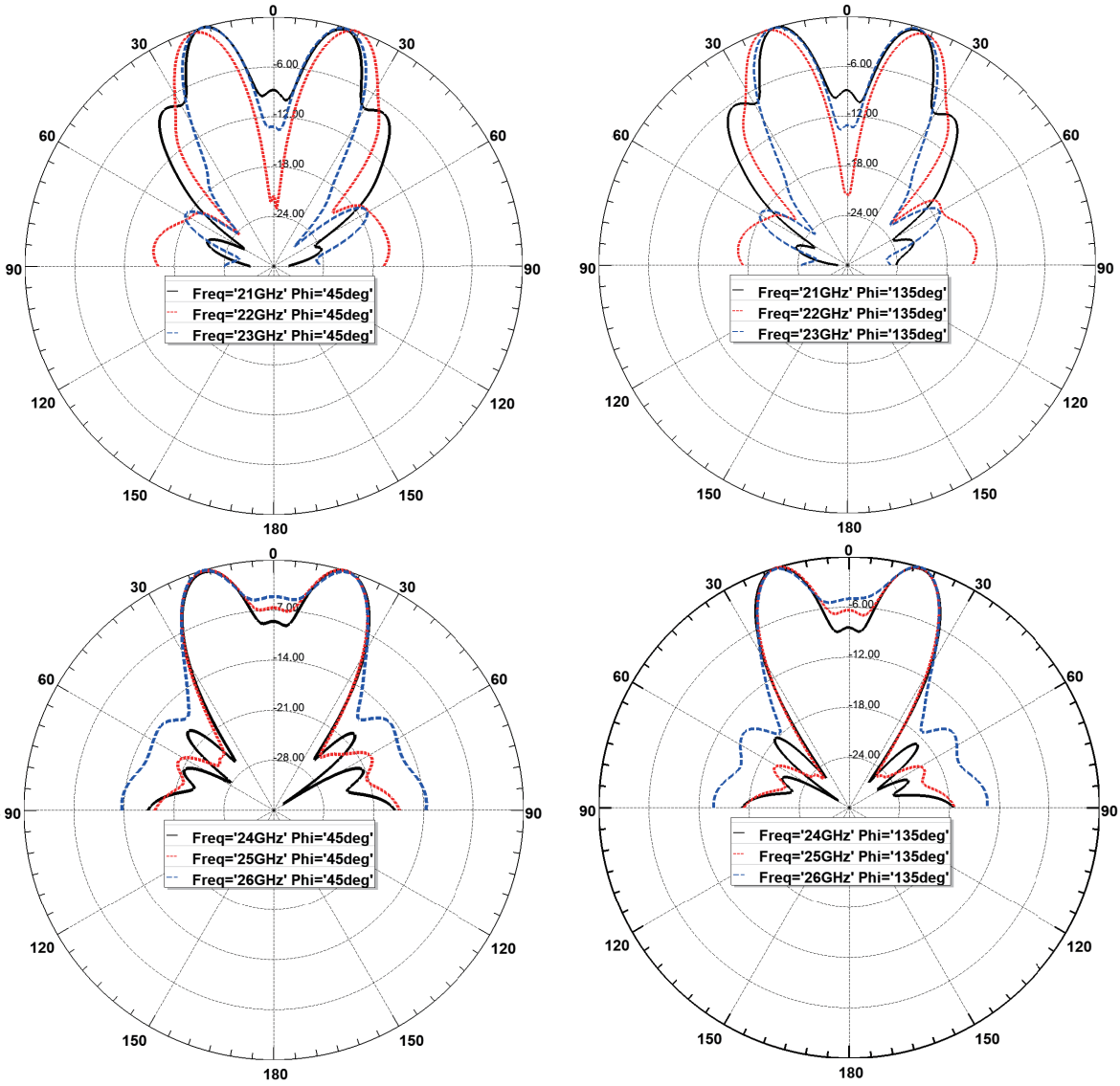


**FIGURE 19**. Normalized radiation pattern at 21, 22, 23, 24, 25, 25, and 26 GHz for mode M2.

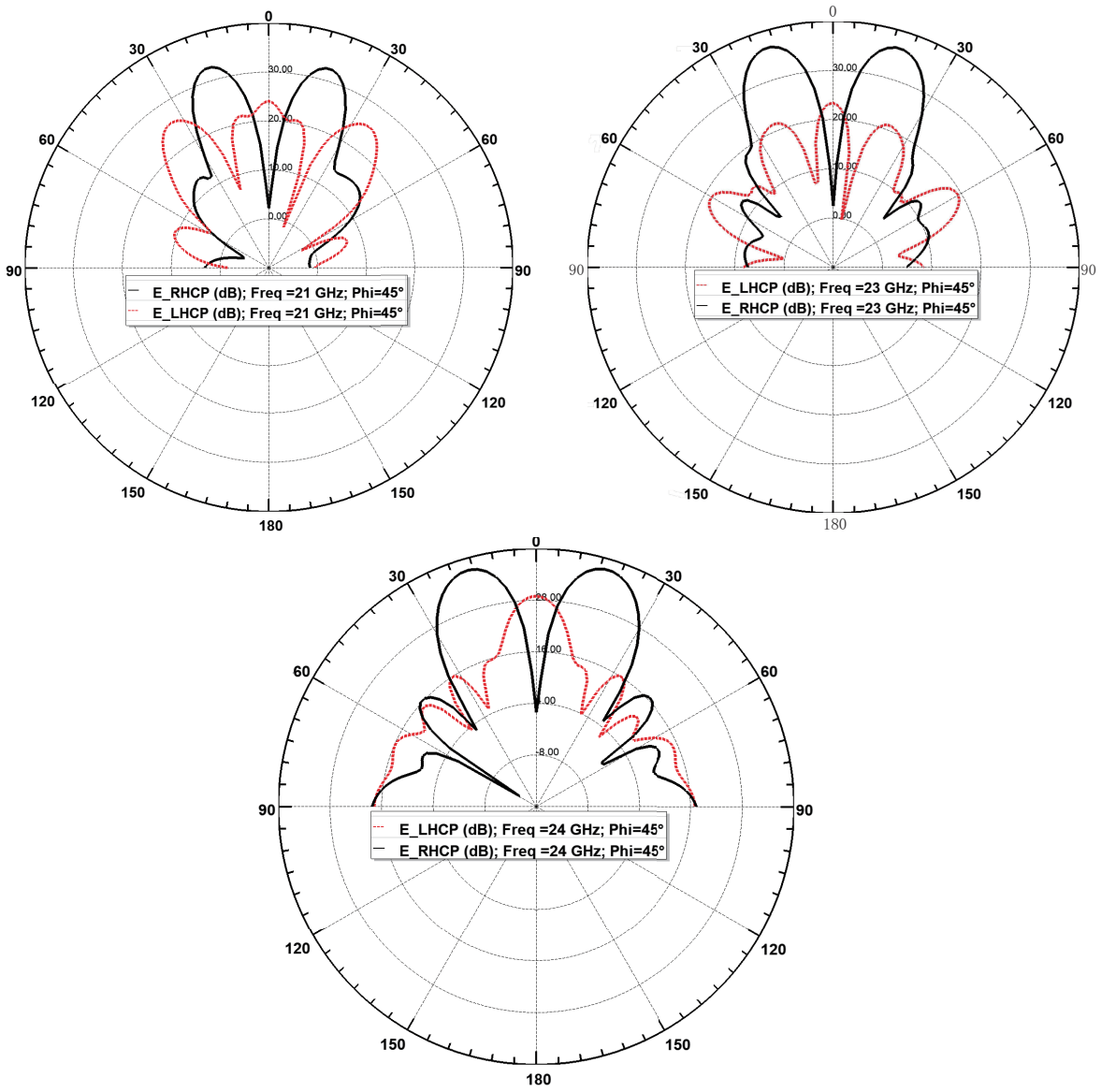


**FIGURE 20**. Cross polar discrimination (XPD) at 21, 23, and 24 GHz for mode M2. The minimum XPD is 22.57 dB at 23 GHz and $\vartheta = 16°$. The antenna is still right-hand circular polarised.

does not influence the polarization sense. Radiated waves are still right-hand circularly polarized with high polarization purity.

Observe that in both operation modes (M1 and M2), the patterns are grating-lobes free, although the antenna is relatively large with 64 elements compared to the operating frequency. The patterns are also stable in the frequency range of interest.

Although the antenna's gain is not a primary concern of the present study, it is nevertheless essential to mention that antenna arrays designed using the technique presented in this work are open to any comparison with comparable antennas in the literature. The $4 \times 4$-DCSA taken here as an example shows a good gain of more than 15 dB over a wide frequency range from 21.36 to 26.89 GHz with a gain of 18.74 dB at the operating frequency and a maximum of 19.89 dB at 25 GHz in mode M1 operation. In mode M2, the gain is above 7.5 dB over a bandwidth of 7.5 GHz, from 19.44 to 26.94 GHz, with a maximum gain of 13.67 at 24 GHz. Remembering that, in mode M2 operation, the antenna radiates four tilted beams simultaneously, and this gain can be considered high.

## 5. CONCLUSION

A simple technique for designing circularly polarized antenna arrays operating in two modes has been presented. A controlled double sequential rotation is used to obtain single and multi-mode radiation in the same frequency range. Proof-of-concept is provided mathematically and through numerical simulations in light of some case studies. Whether operating in single-beam mode or multi-beams, the designed antennas using this technique show overall good radiation characteristics. The approach can not only be applied to large antenna arrays following a modular principle adapted to the array size and needed appli-

cations without loss of generality, but also paves the way for the manufacture of circularly polarized antennas operating in both modes in the same frequency band, thus enabling their use in a wide range of applications, such as:

- monopulse radar systems using a wideband antenna operating in two radiating modes,
- communication and direction-finding systems in civil and military environments,
- compensation of interference and blockage in dynamic communication environments
- satellite communications,
- and radio astronomy.

Moreover, designed antennas using the presented approach can be directly connected to the receiver without a mode-forming network. For simple applications, an hybrid junction is more than enough to make up the sum and the difference in order to obtain a reference pattern (Mode M1) and difference pattern (mode M2) simultaneously. Otherwise, a beam-forming circuit may be needed to allow the vector combination of M1 and M2 modes for a simultaneous radiation of the two modes.

The author would have provided measurement data for comparison. Unfortunately, it was not possible due to a limited budget. Nevertheless, given

a)- the accuracy and precision of the simulations and the consideration of all factors that can influence the radiation characteristics [18, 19],
b)- the fact that the $4 \times 4$ DCSA is based on the $2 \times 2$ DCSA, whose measured and simulated results match [16]. In particular, the $4 \times 4$ DCSA and the $2 \times 2$ DCSA have identical impedance bandwidth,
c)- the certainty that the application of the approach to three different antennas has provided similar results,

there is no doubt that, if carried out, the obtained experimental results will validate simulated data. Potential deviations between measurements and simulated data can be attributed to measurement uncertainties, manufacturing tolerances, inaccuracies in soldering the pin connector, and human-made noise. These sources of errors have already been discussed in [16–19].

Last but not least, if the approach presented here is combined with other methods in the literature, beam steering can be achieved, as will be shown in future work.

## REFERENCES


[1] Huang, J., "A technique for an array to generate circular polarization with linearly polarized elements," *IEEE Transactions on Antennas and Propagation*, Vol. 34, No. 9, 1113–1124, Sep. 1986.

[2] Teshirogi, T., M. Tanaka, and W. Chujo, "Wideband circularly polarized array antenna with sequential rotations and phase shift of elements," *Microstrip Antennas: The Analysis and Design of Microstrip Antennas and Arrays*, 117–120, 1985.

[3] Corzine, R. G. and J. A. Mosko, *Four Arm Spiral Antennas*, Artech House Publishers, 1990.

[4] Hall, P. S. and J. S. Dahele, "Dual and circularly polarized microstrip antennas," *Advances in Microstrip and Printed Antennas*, Vol. 4, 163–222, 1997.

[5] Chen, A., Y. Zhang, Z. Chen, and S. Cao, "A Ka-band high-gain circularly polarized microstrip antenna array," *IEEE Antennas and Wireless Propagation Letters*, Vol. 9, 1115–1118, 2010.

[6] Chen, A., C. Yang, Z. Chen, Y. Zhang, and Y. He, "Design of multilevel sequential rotation feeding networks used for circularly polarized microstrip antenna arrays," *International Journal of Antennas and Propagation*, Vol. 2012, No. 1, 304816, 2012.

[7] Hall, P. S., J. S. Dahele, and J. R. James, "Design principles of sequentially fed, wide bandwidth, circularly polarised microstrip antennas," in *IEE Proceedings H (Microwaves, Antennas and Propagation)*, Vol. 136, No. 5, 381–389, Oct. 1989.

[8] Hall, P. S., "Application of sequential feeding to wide bandwidth, circularly polarised microstrip patch arrays," in *IEE Proceedings H (Microwaves, Antennas and Propagation)*, Vol. 136, No. 5, 390–398, Oct. 1989.

[9] Hall, P. S. and M. S. Smith, "Sequentially rotated arrays with reduced sidelobe levels," *IEE Proceedings — Microwaves, Antennas and Propagation*, Vol. 141, No. 4, 321–325, 1994.

[10] Pouhè, D., "Alternating generation of single and multi-beam modes using the sequential rotation technique in antenna arrays," in *2024 IEEE-APS Topical Conference on Antennas and Propagation in Wireless Communications (APWC)*, 101–105, Lisbon, Portugal, Sep. 2024.

[11] Smith, M. S., "Grating lobes of sequentially rotated antenna arrays," in *1991 Seventh International Conference on Antennas and Propagation, ICAP 91 (IEE)*, 217–220, York, 1991.

[12] Smith, M. S. and P. S. Hall, "Analysis of radiation pattern effects in sequentially rotated arrays," *IEE Proceedings — Microwaves, Antennas and Propagation*, Vol. 141, No. 4, 313–320, 1994.

[13] Zeng, W., X. Y. Wu, F. Wu, Y. Zhang, Z. H. Jiang, W. Hong, and K.-M. Luk, "Broadband dual-CP multi-stage sequential rotation arrays with independent control of polarizations based on dual-CP magnetoelectric dipole elements," *IEEE Transactions on Antennas and Propagation*, Vol. 72, No. 4, 3017–3032, Apr. 2024.

[14] Ma, R. F., Z. H. Jiang, Y. Zhang, X. Y. Wu, T. Yue, W. Hong, and D. H. Werner, "Theory, design, and verification of dual-circularly polarized dual-beam arrays with independent control of polarization: A generalization of sequential rotation arrays," *IEEE Transactions on Antennas and Propagation*, Vol. 69, No. 3, 1369–1382, Mar. 2021.

[15] Karlsson, C., P. Cavero, T. Tekin, and D. Pouhè, "A new broadband antenna for satellite communications," in *2014 IEEE-APS Topical Conference on Antennas and Propagation in Wireless Communications (APWC)*, 800–803, Palm Beach, Aruba, 2014.

[16] Tcheg, P., M. Möck, and D. Pouhè, "An array of double-cornu spiral antenna," *Progress In Electromagnetics Research M*, Vol. 123, 145–151, 2024.

[17] Tcheg, P. and D. Pouhè, "K-band Ka-band planar spiral antenna arrays with integrated corporated feeding network," *Progress In Electromagnetics Research C*, Vol. 113, 227–238, 2021.

[18] Tcheg, P. and D. Pouhè, "A design methodology for the implementation of planar spiral antennas with an integrated corporate feed," *Progress In Electromagnetics Research C*, Vol. 106, 239–253, 2020.

[19] Tcheg, P., M. Möck, and D. Pouhè, "A new broadband antenna of high gain: The double-cornu spiral antenna," *Progress In Electromagnetics Research C*, Vol. 118, 199–212, 2022.